

Rapid emplacement of massive Duluth Complex intrusions within the Midcontinent Rift

Nicholas L. Swanson-Hysell¹, Steven A. Hoaglund², James L. Crowley³, Mark D. Schmitz³, Yiming Zhang¹, James D. Miller Jr.²

¹ Department of Earth and Planetary Science, University of California, Berkeley, CA, USA

² Department of Earth and Environmental Sciences, University of Minnesota, Duluth, MN, USA

³ Department of Geosciences, Boise State University, Boise, ID, USA

This article is to be submitted for consideration at GEOLOGY (published by the Geological Society of America).

¹ ABSTRACT

The Duluth Complex is one of the largest mafic intrusive complexes in the world. It was emplaced as the Midcontinent Rift developed in Laurentia's interior during an interval of magmatism and extension from *ca.* 1109 to 1084 Ma. This duration of magmatic activity is more protracted than is typical for large igneous provinces interpreted to have resulted from decompression melting of upwelling mantle plumes. While the overall duration of magmatic activity was protracted, there were intervals of more voluminous magmatism. High-precision U-Pb geochronology can give insight into the timescale of these pulses. Paleomagnetic data can also give chronological constraints for rocks of the Midcontinent Rift given the large change in paleolatitude that occurred over the interval of rift magmatism. In this work, we present new high-precision $^{206}\text{Pb}/^{238}\text{U}$ dates for both the anorthositic and layered series of the Duluth Complex and demonstrate that they were both emplaced during a <1 million year long interval *ca.* 1096 Ma. Comparison of compiled and new paleomagnetic data from these units with the chronostratigraphically-constrained apparent polar wander path supports this interpretation.

15 This timing of emplacement corresponds with eruptions of the North Shore Volcanic Group. The
16 rapid emplacement of Duluth Complex intrusions and North Shore Volcanic Group lavas bears
17 similarities to the geologically short duration of well-dated large igneous provinces. These data
18 support hypotheses that call upon the co-location of magmatism and rifting as the result of
19 lithospheric extension atop decompression melting of anomalous hot upwelling mantle. This rapid
20 magmatic pulse occurred more than 10 million years after initial magmatic activity following
21 more than 20° of latitudinal plate motion. A likely scenario is one in which upwelling mantle flow
22 spread across the base of Laurentian lithosphere resulting in the southwest Laurentia large
23 igneous provinces while flowing upwards to the rift via “upside-down drainage.”

24 INTRODUCTION

25 The Midcontinent Rift represents a protracted tectonomagmatic event in the interior of the
26 Laurentia (the North American craton). Voluminous outpouring of lava and emplacement of
27 intrusions accompanied rift development (Fig. 1). Magmatic activity initiated *ca.* 1109 Ma and
28 continued until *ca.* 1084 Ma (Swanson-Hysell et al., 2019). Preserved thicknesses for volcanic
29 successions range from nearly 10 km for the partial sections exposed on land, such along the
30 North Shore of Minnesota (Green et al., 2011), up to ~25 km interpreted to be preserved under
31 Lake Superior (Cannon, 1992). These volcanics and associated intrusions are much more
32 voluminous than is typical for a tectonic rifting event. Analysis of seismic data leads to a
33 preserved volcanic volume estimate of $1.5 \times 10^6 \text{ km}^3$ (Cannon, 1992). Total eruptive volume is
34 estimated to have exceeded $2 \times 10^6 \text{ km}^3$ and there are indications of a much greater volume
35 having been added to the lithosphere as intrusions and an underplate (Cannon, 1992). The
36 duration of volcanism of ~25 Myr in the Midcontinent Rift is much longer than is typical for
37 large igneous province emplacement associated with decompression melting of an upwelling
38 mantle plume. Well-dated large igneous provinces, such as the Central Atlantic Magmatic
39 Province (Blackburn et al., 2013), the Karoo-Ferrar (Burgess et al., 2015), and the Deccan Traps

(Schoene et al., 2019; Sprain et al., 2019) have much shorter durations of <1 Myr for the bulk of their magmatic activity. An explanation for prolonged volcanism in the Midcontinent Rift could attribute rift initiation and initial volcanism via plume arrival with continued volcanism resulting from rift-driven asthenospheric upwelling. However, the most voluminous period of magmatism occurred more than 10 million years after initial flood volcanism during an interval known as the “main magmatic stage” (Vervoort et al., 2007).

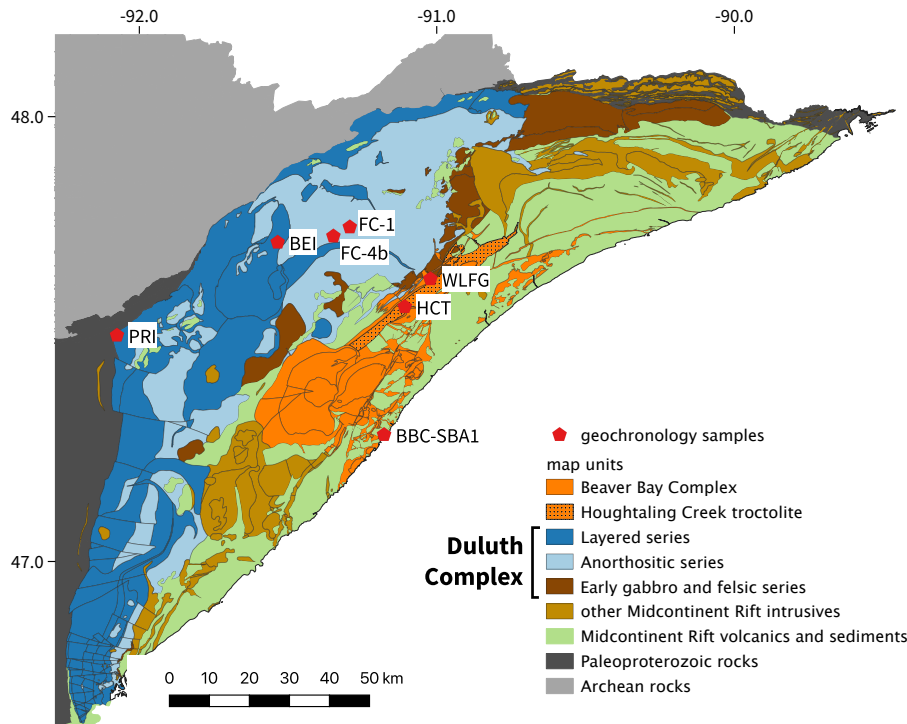


Figure 1. Geologic map of northeastern Minnesota (simplified from Jirsa et al., 2011) highlighting the extent of the major intrusive complexes of the Midcontinent Rift and showing the geochronology sample locations. The older Felsic series and Early Gabbro series of the Duluth Complex are grouped as the “Early series.” Dates from the anorthositic and layered series of the Duluth Complex (shown in light and dark blue) indicate rapid emplacement in less than 1 million years.

Pioneering Midcontinent Rift geochronology utilized $^{207}\text{Pb}/^{206}\text{Pb}$ dates on zircon from both extrusive volcanics (Davis and Green, 1997) and intrusions (Paces and Miller, 1993) to illuminate this prolonged history of magmatism and interpret periods of enhanced activity. Subsequent advances in U-Pb geochronology enable higher precision $^{206}\text{Pb}/^{238}\text{U}$ dates to be used when dates have been developed utilizing chemical abrasion methods that mitigate Pb-loss (Mattinson, 2005). Such dates can be compared at the level of analytical uncertainty when they have been developed using the EARTHTIME tracer (Condon et al., 2015). An updated chronostratigraphic framework for Midcontinent Rift volcanics was recently published (Swanson-Hysell et al., 2019) that included

54 new U-Pb dates developed using these methods (Fig. 2). With these higher precision constraints,
55 the timing and tempo of magmatic activity within the rift can be reevaluated. Of particular
56 interest is whether magmatic activity was continuous or punctuated by pulses. Key to evaluating
57 this question is the timing of emplacement of intrusive rocks throughout the Midcontinent Rift
58 particularly the largest one – the Duluth Complex (Fig. 1). The Duluth Complex is the largest
59 intrusive complex in the Midcontinent Rift. With its arcuate area of 5630 km², the Duluth
60 Complex constitutes the second-largest exposed mafic intrusive complex in the world, with only
61 the Bushveld Complex of South Africa being larger (Miller et al., 2002). The tholeiitic Duluth
62 Complex was emplaced as sheet-like intrusions into the base of the comagmatic volcanic
63 succession with the majority of its volume associated with the anorthositic series and the layered
64 series of gabbroic and troctolitic cumulates (Miller et al., 2002; Fig. 1). In this work, we present
65 ²⁰⁶Pb/²³⁸U dates from the Duluth Complex, as well as the Beaver Bay Complex, to establish the
66 duration of Duluth Complex magmatism and contextualize it with the chronology of rift
67 volcanism.

68 METHODS and RESULTS

69 U-Pb geochronology methods for isotope dilution thermal ionization mass spectrometry
70 (ID-TIMS) follow Schmitz (2012). Single zircon crystals were chemically abraded prior to analysis
71 in the Boise State Isotope Geology Laboratory. Weighted means were calculated from multiple
72 single zircon dates with some dates being excluded due to Pb-loss (Fig. 2 and Table 1).¹
73 Uncertainties for the weighted mean dates are given as ±X/Y/Z in Table 1, where X is the
74 analytical uncertainty, Y is the combined analytical and tracer uncertainty, and Z is the combined
75 analytical, tracer and ²³⁸U decay constant uncertainty (0.108%; Jaffey et al., 1971). This Z error
76 needs to be utilized when comparing to dates developed using other decay systems (e.g.,

¹GSA Data Repository item 2020XXX, table of individual zircon dates is available online at <http://www.geosociety.org/datarerepository>. All paleomagnetic data and interpreted specimen directions are available to the measurement level in the MagIC database (<https://earthref.org/MagIC/doi/>). All code associated with statistical tests and data visualization is available within a Zenodo repository.

⁷⁷ $^{40}\text{Ar}/^{39}\text{Ar}$, $^{187}\text{Re}-^{187}\text{Os}$). Given that the focus in this work is comparing these dates to one
⁷⁸ another, and to other $^{206}\text{Pb}/^{238}\text{U}$ dates developed using EARTHTIME tracer solutions (e.g.
⁷⁹ Swanson-Hysell et al., 2019), the X error will be referred to when the results are reported and
⁸⁰ discussed in the text.

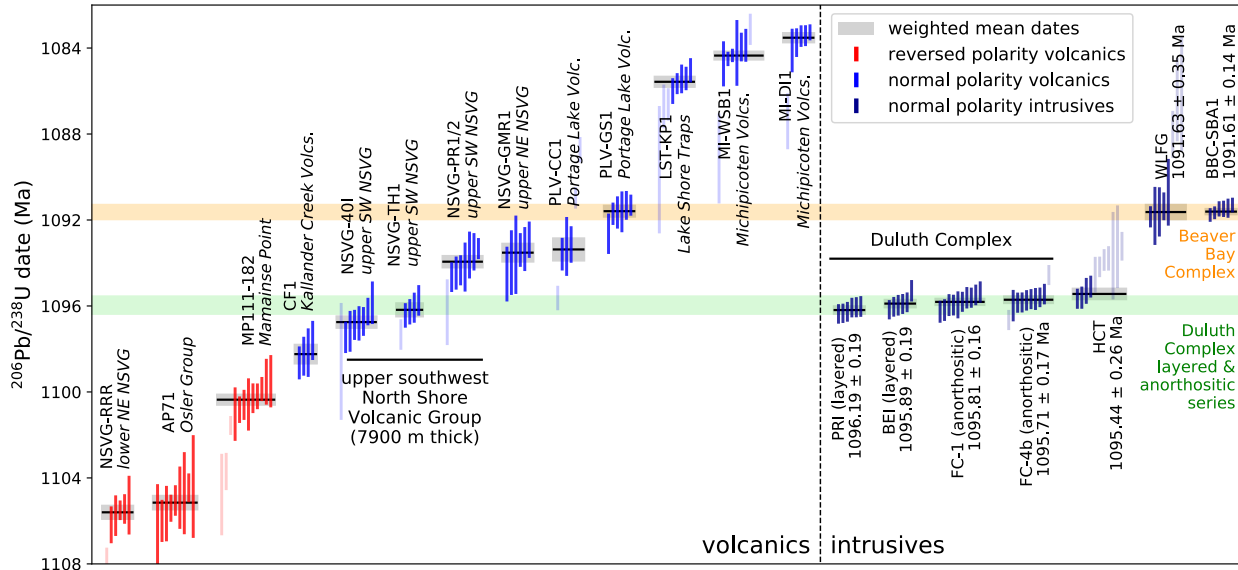


Figure 2. Date bar plot of CA-ID-TIMS $^{206}\text{Pb}/^{238}\text{U}$ dates for Midcontinent Rift volcanics and intrusives. Each vertical bar represents the date for an individual zircon (colored by the magnetic polarity of the unit) while the horizontal lines and grey boxes represent the weighted means and their uncertainty. The green horizontal bar represents the interval of emplacement of the layered and anorthositic series of the Duluth Complex. The orange horizontal bar represents the interval of Beaver Bay Complex magmatism represented by the Wilson Lake Ferrogabbro and the Silver Bay intrusions.

⁸¹ The Duluth Complex anorthositic series comprises plagioclase-rich gabbroic cumulates varying
⁸² from anorthositic gabbro to anorthosite. Samples FC-1 and FC-4b are of gabbroic anorthosite
⁸³ collected from exposures near the former logging town of Forest Center. Zircon grains from these
⁸⁴ samples are commonly used as laser ablation U-Pb geochronology standards. A weighted mean
⁸⁵ $^{206}\text{Pb}/^{238}\text{U}$ date for FC-1 of 1095.81 ± 0.16 Ma is calculated based on 10 single zircon dates
⁸⁶ (Table 1). The FC-4b date is indistinguishable from FC-1 with a weighted mean $^{206}\text{Pb}/^{238}\text{U}$ date
⁸⁷ of 1095.71 ± 0.17 Ma based on dates from 8 zircons.

⁸⁸ The layered series of the Duluth Complex is a suite of stratiform troctolitic to gabbroic

Table 1. Summary of CA-ID-TIMS $^{206}\text{Pb}/^{238}\text{U}$ dates from Midcontinent Rift intrusions

Sample	Group	Latitude Longitude	$^{206}\text{Pb}/^{238}\text{U}$ date (Ma)	Error (2σ)			MSWD	n
				X	Y	Z		
PRI <i>Partridge River intrusion</i>	Duluth Complex layered series	47.5480°N 92.1074°W	1096.19	0.19	0.36	1.15	0.45	6
BEI <i>Bald Eagle intrusion</i>	Duluth Complex layered series	47.7516°N 91.5680°W	1095.89	0.19	0.36	1.15	1.59	6
FC-1 <i>Forest Center anorthosite</i>	Duluth Complex anorthositic series	47.7827°N 91.3266°W	1095.81	0.16	0.34	1.14	1.44	10
FC-4b <i>Forest Center anorthosite</i>	Duluth Complex anorthositic series	47.7677°N 91.3753°W	1095.71	0.17	0.35	1.14	0.38	8
HCT <i>Houghtaling Creek troctolite</i>	Beaver Bay Complex	47.6009°N 91.1497°W	1095.44	0.26	0.40	1.16	1.13	4
WLFG <i>Wilson Lake ferrogabbro</i>	Beaver Bay Complex	47.6620°N 91.0619°W	1091.63	0.35	0.46	1.18	0.74	5
BBC-SBA1 <i>Silver Bay aplite</i>	Beaver Bay Complex	47.6620°N 91.0619°W	1091.61	0.14	0.30	1.2	1.0	6

Notes: X—internal (analytical) uncertainty in the absence of external or systematic errors; Y—uncertainty incorporating the U-Pb tracer calibration error; Z—uncertainty including X and Y, as well as decay constant uncertainty; MSWD—mean square of weighted deviates; n—number of individual zircon dates included in the calculated sample mean date. All dates are from this study with the exception of BBC-SBA1 which was published in Fairchild et al. (2017). Data for individual zircons are provided in the Data Repository.

89 cumulates that were emplaced as discrete layered intrusions (Fig. 1). The PRI sample is a
 90 coarse-grained augite troctolite from the Partridge River intrusion which is at the base of the
 91 complex in contact with underlying Paleoproterozoic metasedimentary rocks (Fig. 1). Data from
 92 6 zircons result in a weighted mean $^{206}\text{Pb}/^{238}\text{U}$ date of 1096.19 ± 0.19 Ma (Fig. 2). The BEI
 93 sample is a coarse-grained olivine gabbro from the Bald Eagle intrusion. This intrusion has been
 94 interpreted to be one of the youngest layered series units based on cross-cutting relationships
 95 inferred from aeromagnetic data (Miller et al., 2002). Dates from 6 zircons of the BEI sample
 96 result in a weighted mean $^{206}\text{Pb}/^{238}\text{U}$ date of 1095.89 ± 0.19 Ma (Fig. 2) that is indistinguishable
 97 from the anorthositic series FC-1 and FC-4b dates.

98 The Beaver Bay complex is a suite of dominantly hypabyssal (emplaced at shallow depth)
 99 intrusions that cross-cut the North Shore Volcanic Group (Fig. 1). Sample HCT is an augite
 100 troctolite from the Houghtaling Creek troctolite. The Houghtaling Creek troctolite comprises
 101 medium-grained olivine-plagioclase cumulates interpreted to have been emplaced as a macrodike
 102 (Miller et al., 2001). While some zircons from HCT have Pb-loss that was not fully mitigated by
 103 chemical abrasion, dates from 4 concordant zircons result in a weighted mean $^{206}\text{Pb}/^{238}\text{U}$ date of

104 1095.44 ± 0.26 Ma (Fig. 2). A sample of coarse-grained ferrodiorite was collected as WLFG from
 105 the Wilson Lake ferrogabbro of the Beaver Bay Complex. The Wilson Lake ferrogabbro is a
 106 plug-shaped zoned intrusion that was emplaced into the roof zone of the Duluth Complex. Dates
 107 from 5 zircons result in a weighted mean $^{206}\text{Pb}/^{238}\text{U}$ date of 1091.63 ± 0.35 Ma (Fig. 2). This
 108 date overlaps within uncertainty with the $^{206}\text{Pb}/^{238}\text{U}$ date of 1091.61 ± 0.14 Ma from an aplite
 109 within a Silver Bay intrusion of the Beaver Bay Complex (Fairchild et al., 2017; Figs. 1 and 2).

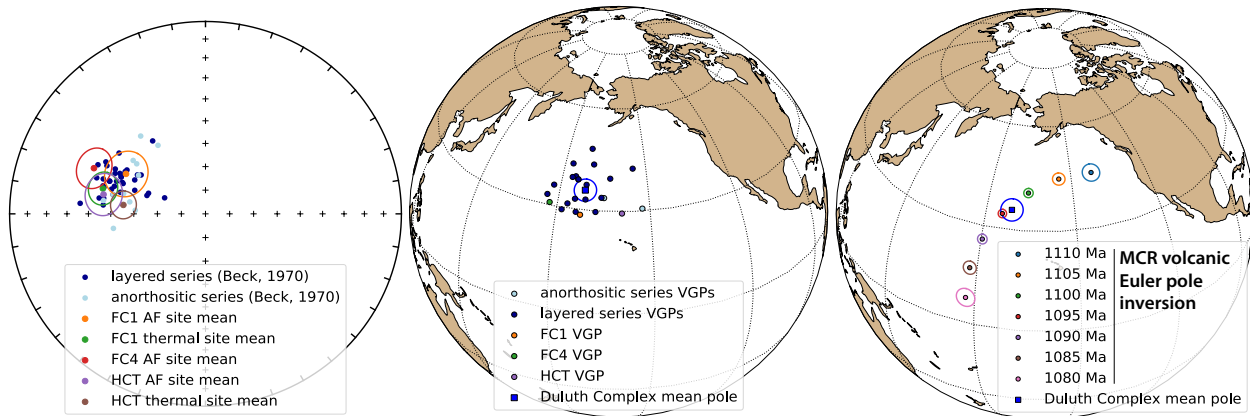


Figure 3. Left panel: tilt-corrected site mean paleomagnetic directions from anorthositic and layered series sites of Beck (1970) in the vicinity of Duluth. Center panel: Virtual geomagnetic poles (VGPs) from Duluth-vicinity sites with $\alpha_{95} < 15^\circ$ and from the FC1, FC4 and HCT sites give a mean pole of: 188.7°E , 35.6°N , $N=24$, $A_{95}=3.1$, $k=92$. Right panel: Duluth Complex paleomagnetic pole shown with a synthesized pole path developed using an Euler pole inversion of chronostratigraphically-constrained Midcontinent Rift volcanic poles (Swanson-Hysell et al., 2019).

110 Paleomagnetic data from Midcontinent Rift intrusions throughout northeastern Minnesota,
 111 including the Duluth Complex, were published in Beck (1970). These data include many sites
 112 from the layered series (37 sites) and anorthositic series (11 sites) collected in the vicinity of the
 113 city of Duluth (Fig. 3). Statistical tests show the site directions of the layered and anorthositic
 114 series to share a common mean, consistent with their similar U-Pb dates. In order to have
 115 paleomagnetic data directly paired with the geochronology, oriented cores were collected and
 116 analyzed from the sites of the FC-1, FC-4 and HCT samples. Magnetization was measured on a
 117 2G DC-SQUID magnetometer in the UC Berkeley paleomagnetism lab. Following the
 118 measurement of natural remanent magnetization, the samples underwent alternating field or
 119 thermal demagnetization steps. Fits were made using the PmagPy software (Tauxe et al., 2016).

120 While Beck (1970) did not discuss or implement tilt corrections, the Duluth Complex and
121 overlying lava flows gently dip towards Lake Superior. The paleomagnetic sites need to be
122 tilt-corrected to the inferred paleohorizontal to properly interpret the paleomagnetic directions.
123 We compiled abundant igneous layering orientation measurements, which are similar to the
124 orientations of overlying lavas and interflow sediments, and use them for tilt-correction.

125 The rapid progression of poles within the apparent polar wander path (APWP) of the
126 Midcontinent Rift enable these paleomagnetic data to give chronological insight. The positions of
127 poles from the early stage of rift magmatism are quite different from main stage lavas (Fig. 3).
128 The similar position of virtual geomagnetic poles (VGPs) from across the Duluth Complex
129 layered and anorthositic series, including the FC sites, is consistent with contemporaneous
130 emplacement and they can be combined into a mean pole (Fig. 3). This paleomagnetic pole can
131 be compared to a synthesized Midcontinent Rift APWP developed using an Euler pole inversion
132 to chronostratigraphically-constrained volcanic poles (Swanson-Hysell et al., 2019). The Duluth
133 Complex pole lies between the 1100 Ma to 1095 Ma path positions with the A_{95} uncertainty of
134 the pole overlapping with the two angular standard deviations ellipse of the 1095 Ma pole
135 position. This result is consistent with a *ca.* 1096 Ma age for the layered and anorthositic series of
136 the Duluth Complex while strengthening the correlation with the volcanics.

137 DISCUSSION

138 The new U-Pb dates, together with the paleomagnetic data, imply that the bulk of both the
139 layered series and the anorthositic series of the Duluth Complex were emplaced in less than
140 900,000 years between *ca.* 1096.4 and 1095.5 Ma (Fig. 2). Comparison with geochronology from
141 Midcontinent Rift volcanics demonstrates that this emplacement was coeval with eruption of the
142 upper southeast sequence of the North Shore Volcanic Group (NSVG) which comprises ~7900
143 meters of lavas and is the thickest exposed Midcontinent Rift volcanic succession. The
144 indistinguishable ages of the anorthositic and layered series of the Duluth Complex, together with

145 coeval NSVG eruptions, indicate that *ca.* 1096 Ma there was a large pulse of melt generation.

146 The 1095.44 ± 0.26 Ma age of the Houghtaling Creek troctolite is indistinguishable from the
147 younger Duluth Complex dates. This result indicates that this pulse of voluminous magmatic
148 activity is represented in some intrusions within the Beaver Bay Complex. As the NSVG
149 thickened, the intrusive horizon migrated upwards including the major Houghtaling Creek
150 macrodike. A younger pulse of Beaver Bay Complex magmatism postdates NSVG eruptions as
151 units such as the Beaver River diabase and the Silver Bay intrusions penetrate the youngest
152 NSVG lavas, including the 1093.94 ± 0.28 Ma Palisade Rhyolite (Miller et al., 2001;
153 Swanson-Hysell et al., 2019; Fig. 1). The age of this magmatism is represented by the
154 indistinguishable dates of 1091.63 ± 0.35 Ma for the Wilson Lake ferrogabbro and 1091.61 ± 0.14
155 Ma from the Silver Bay intrusions (Fig. 2; Table 1). This younger Beaver Bay Complex
156 magmatism is coeval with the eruption of the more than >5 km thick Portage Lake Volcanics
157 that are exposed on the Keweenaw Peninsula and on Isle Royale (Fig. 2).

158 Rapid emplacement of the voluminous layered and anorthositic series of the Duluth Complex
159 bears similarities to the geologically short duration (<1 Myr) of well-dated continental flood
160 basalt provinces (Burgess et al., 2015; Schoene et al., 2019). This similarity supports the
161 hypothesis put forwarded by Green (1983), and advanced by others including Cannon and Hinze
162 (1992) and Stein et al. (2015), that the co-location of massive magmatism and rifting is the result
163 of lithospheric extension atop decompression melting of an upwelling mantle plume. Heating of
164 Laurentia lithosphere at the time 600 km to the north of the rift is indicated by
165 thermochronologic data from middle to lower crustal xenoliths (Edwards and Blackburn, 2018).
166 Basaltic magma was also emplaced throughout the Southwest large igneous province coeval with
167 the Midcontinent Rift, including sills more than 2300 km from Duluth (Bright et al., 2014). That
168 such a broad region of Laurentia lithosphere experienced heating and magmatism supports the
169 interpretation that large-scale mantle upwelling was a driver of melt generation.

170 Both the *ca.* 1108 early stage and *ca.* 1096 Ma main stage volcanism within the Midcontinent

Rift was voluminous and interpreted to be the result of a plume-related thermal anomaly. The interpretation that this volcanism is associated with a deep-seated mantle plume needs to be reconciled with both the long duration and the record of rapid equatorward motion of North America from a latitude of $\sim 54^{\circ}\text{N}$ *ca.* 1108 Ma during early stage flood basalt eruptions to $\sim 32^{\circ}\text{N}$ by *ca.* 1096 Ma main stage volcanism (paleolatitudes for the location of Duluth, MN). While some of this motion could be associated with true polar wander, in which the mesosphere and asthenosphere rotated in conjunction with the lithosphere, Swanson-Hysell et al. (2019) showed that the record of paleomagnetic poles requires a substantial component of differential plate tectonic motion. The pulsed nature of magmatic activity could support a model wherein there were multiple upwelling pulses. As postulated by Cannon and Hinze (1992), the initial pulse that was expressed by *ca.* 1108 early stage volcanism could have initiated lithospheric thinning. Given significant lithospheric thinning in the Midcontinent Rift region, subsequent positively-buoyant plume material that encountered Laurentia lithosphere would have experienced “upside-down” drainage wherein relief at the base of the lithosphere resulted in lateral and upward flow into the Midcontinent Rift (Sleep, 1997; Swanson-Hysell et al., 2014). One scenario is that Laurentia was migrating over a plume generation zone (Burke et al., 2008) from which multiple deep-seated mantle plumes upwelled to the lithosphere over that time interval. The first could have been centered on the Midcontinent Rift with the second encountering Laurentian lithosphere and being directed to the rift by upside-down drainage in addition to driving magmatism in southwest Laurentia. Another scenario is that *ca.* 1096 Ma magmatism was invigorated by upwelling return flow enhanced by slab avalanche induced downwelling connected to the rapid plate motion of Laurentia that initiated in the early history of rift development (Swanson-Hysell et al., 2019). Overall, the constraint that both the anorthositic and layered series of the Duluth Complex were emplaced in less than 1 million years requires an exceptional thermal anomaly that lead to voluminous rapid melt generation during the main stage of Midcontinent Rift development.

196 ACKNOWLEDGEMENTS

197 Project research was supported by NSF EAR-1847277 (awarded to NLS-H) and the University of
198 Minnesota, Duluth Earth and Environmental Sciences. Funding for the analytical infrastructure
199 of the Boise State University Isotope Geology Laboratory was provided by NSF EAR-0824974
200 and EAR-0521221. Margaret Avery and Dan Costello provided field assistance. Debbie Pierce
201 assisted with analyses in the Boise State Isotope Geology Laboratory.

202 REFERENCES

- 203 Beck, M., 1970, Paleomagnetism of Keweenawan intrusive rocks, Minnesota: *Journal of Geophysical Research*,
204 vol. 75, pp. 4985–4996, doi:10.1029/JB075i026p04985.
- 205 Blackburn, T. J., Olsen, P. E., Bowring, S. A., McLean, N. M., Kent, D. V., Puffer, J., McHone, G., Rasbury, E. T.,
206 and Et-Touhami, M., 2013, Zircon U-Pb geochronology links the end-Triassic extinction with the Central
207 Atlantic Magmatic Province: *Science*, vol. 340, pp. 941–945, doi:10.1126/science.1234204.
- 208 Bright, R. M., Amato, J. M., Denyszyn, S. W., and Ernst, R. E., 2014, U-Pb geochronology of 1.1 Ga diabase in the
209 southwestern United States: Testing models for the origin of a post-Grenville large igneous province:
210 *Lithosphere*, vol. 6, pp. 135–156, doi:10.1130/L335.1.
- 211 Burgess, S. D., Bowring, S. A., Fleming, T. H., and Elliot, D. H., 2015, High-precision geochronology links the
212 Ferrar large igneous province with early-Jurassic ocean anoxia and biotic crisis: *Earth and Planetary Science
Letters*, vol. 415, pp. 90–99, doi:10.1016/j.epsl.2015.01.037.
- 213 Burke, K., Steinberger, B., Torsvik, T. H., and Smethurst, M. A., 2008, Plume generation zones at the margins of
214 large low shear velocity provinces on the core–mantle boundary: *Earth and Planetary Science Letters*, vol. 265,
215 pp. 49–60, doi:10.1016/j.epsl.2007.09.042.
- 216 Cannon, W. F., 1992, The Midcontinent rift in the Lake Superior region with emphasis on its geodynamic
217 evolution: *Tectonophysics*, vol. 213, pp. 41–48, doi:10.1016/0040-1951(92)90250-A.
- 218 Cannon, W. F. and Hinze, W. J., 1992, Speculations on the origin of the North American Midcontinent rift:
219 *Tectonophysics*, vol. 213, pp. 49–55, doi:10.1016/0040-1951(92)90251-Z.
- 220 Condon, D. J., Schoene, B., McLean, N. M., Bowring, S. A., and Parrish, R. R., 2015, Metrology and traceability of
221 U–Pb isotope dilution geochronology (EARTHTIME tracer calibration part I): *Geochimica et Cosmochimica
Acta*, vol. 164, pp. 464–480, doi:10.1016/j.gca.2015.05.026.
- 222 Davis, D. and Green, J., 1997, Geochronology of the North American Midcontinent rift in western Lake Superior
223 and implications for its geodynamic evolution: *Canadian Journal of Earth Science*, vol. 34, pp. 476–488,
224 doi:10.1139/e17-039.
- 225 Edwards, G. H. and Blackburn, T., 2018, Detecting the extent of ca. 1.1 Ga Midcontinent Rift plume heating using
226 U-Pb thermochronology of the lower crust: *Geology*, vol. 46, pp. 911–914, doi:10.1130/g45150.1.
- 227 Fairchild, L. M., Swanson-Hysell, N. L., Ramezani, J., Sprain, C. J., and Bowring, S. A., 2017, The end of
228 Midcontinent Rift magmatism and the paleogeography of Laurentia: *Lithosphere*, vol. 9, pp. 117–133,
229 doi:10.1130/L580.1.

- 232 Green, J., 1983, Geologic and geochemical evidence for the nature and development of the Middle Proterozoic
233 (Keweenawan) Midcontinent Rift of North America: *Tectonophysics*, vol. 94, pp. 413–437,
234 doi:10.1016/0040-1951(83)90027-6.
- 235 Green, J. C., Boerboom, T. J., Schmidt, S. T., and Fitz, T. J., 2011, The North Shore Volcanic Group:
236 Mesoproterozoic plateau volcanic rocks of the Midcontinent Rift System in northeastern Minnesota: *GSA Field
237 Guides*, vol. 24, pp. 121–146, doi:10.1130/2011.0024(07).
- 238 Jaffey, A., Flynn, K., Glendenin, L., Bentley, W., and Essling, A., 1971, Precision measurement of half-lives and
239 specific activities of ^{235}U and ^{238}U : *Physical Review*, vol. C4, pp. 1889–1906, doi:10.1103/PhysRevC.4.1889.
- 240 Jirsa, M. A., Boerboom, T., Chandler, V., Mossler, J., Runkel, A., and Setterholm, D., 2011, S-21 Geologic map of
241 Minnesota-bedrock geology: Tech. rep., Minnesota Geological Survey, URL
242 <http://hdl.handle.net/11299/101466>.
- 243 Mattinson, J. M., 2005, Zircon U/Pb chemical abrasion (CA-TIMS) method: Combined annealing and multi-step
244 partial dissolution analysis for improved precision and accuracy of zircon ages: *Chemical Geology*, vol. 220, pp.
245 47–66, doi:10.1016/j.chemgeo.2005.03.011.
- 246 Miller, J., James D., Green, J. C., Severson, M. J., Chandler, V. W., and Peterson, D. M., 2001, M-119 Geologic
247 map of the Duluth Complex and related rocks, northeastern Minnesota: Tech. rep., Minnesota Geological Survey.
- 248 Miller, J., J.D., Green, J., Severson, M., Chandler, V., Hauck, S., Peterson, D., and Wahl, T., 2002, Geology and
249 mineral potential of the Duluth Complex and related rocks of northeastern Minnesota: Minnesota Geological
250 Survey Report of Investigations, vol. 58.
- 251 Paces, J. and Miller, J., 1993, Precise U-Pb ages of Duluth Complex and related mafic intrusions, northeastern
252 Minnesota: Geochronological insights to physical, petrogenetic, paleomagnetic and tectonomagmatic processes
253 associated with the 1.1 Ga Midcontinent Rift System: *Journal of Geophysical Research*, vol. 98, pp.
254 13,997–14,013, doi:10.1029/93jb01159.
- 255 Schmitz, M. D., 2012, The Geologic Time Scale, Elsevier, Boston, chap. 6 – Radiogenic Isotope Geochronology, pp.
256 115–126: doi:10.1016/B978-0-444-59425-9.00006-8.
- 257 Schoene, B., Eddy, M. P., Samperton, K. M., Keller, C. B., Keller, G., Adatte, T., and Khadri, S. F. R., 2019, U-Pb
258 constraints on pulsed eruption of the Deccan Traps across the end-Cretaceous mass extinction: *Science*, vol. 363,
259 pp. 862–866, doi:10.1126/science.aau2422.
- 260 Sleep, N. H., 1997, Lateral flow and ponding of starting plume material: *Journal of Geophysical Research: Solid
261 Earth*, vol. 102, pp. 10,001–10,012, doi:10.1029/97JB00551.
- 262 Sprain, C. J., Renne, P. R., Vanderkluysen, L., Pande, K., Self, S., and Mittal, T., 2019, The eruptive tempo of
263 Deccan volcanism in relation to the Cretaceous-Paleogene boundary: *Science*, vol. 363, pp. 866–870,
264 doi:10.1126/science.aav1446.
- 265 Stein, C. A., Kley, J., Stein, S., Hindle, D., and Keller, G. R., 2015, North America's Midcontinent Rift: When rift
266 met LIP: *Geosphere*, doi:10.1130/GES01183.1.
- 267 Swanson-Hysell, N. L., Ramezani, J., Fairchild, L. M., and Rose, I. R., 2019, Failed rifting and fast drifting:
268 Midcontinent Rift development, Laurentia's rapid motion and the driver of Grenvillian orogenesis: *GSA Bulletin*,
269 doi:10.1130/b31944.1.
- 270 Swanson-Hysell, N. L., Vaughan, A. A., Mustain, M. R., and Asp, K. E., 2014, Confirmation of progressive plate
271 motion during the Midcontinent Rift's early magmatic stage from the Osler Volcanic Group, Ontario, Canada:
272 *Geochemistry Geophysics Geosystems*, vol. 15, pp. 2039–2047, doi:10.1002/2013GC005180.

- 273 Tauxe, L., Shaar, R., Jonestrask, L., Swanson-Hysell, N., Minnett, R., Koppers, A., Constable, C., Jarboe, N.,
274 Gaastra, K., and Fairchild, L., 2016, PmagPy: Software package for paleomagnetic data analysis and a bridge to
275 the Magnetics Information Consortium (MagIC) Database: *Geochemistry, Geophysics, Geosystems*,
276 doi:10.1002/2016GC006307.
- 277 Vervoort, J., Wirth, K., Kennedy, B., Sandland, T., and Harpp, K., 2007, The magmatic evolution of the
278 Midcontinent rift: New geochronologic and geochemical evidence from felsic magmatism: *Precambrian Research*,
279 vol. 157, pp. 235–268, doi:10.1016/j.precamres.2007.02.019.

Table DR1. Zircon chemical abrasion IDTIMS U-Pb isotopic data

280	Sample	Compositional Parameters						Radiogenic Isotope Ratios						Isotopic Ages					
		I _{th}	²⁰⁶ Pb*	mol %	Pb*	Pb _c	²⁰⁶ Pb	²⁰⁸ Pb	²⁰⁷ Pb	²⁰⁷ Pb	²⁰⁶ Pb	corr.	²⁰⁷ Pb	²⁰⁷ Pb	²⁰⁶ Pb				
		U	x10 ⁻¹³ mol	(c)	Pb _b	(pg)	²⁰⁴ Pb	²⁰⁵ Pb	²⁰⁶ Pb	²⁰⁷ Pb	²³⁵ U	coef.	²⁰⁶ Pb	²³⁵ U	²³⁸ U	²⁰⁶ Pb			
<i>PRI Partridge River intrusion</i> (Duluth Complex layered series)																			
z2	0.665	20.7388	0.9995	599	0.91	34763	0.201	0.0761152	0.042	1.94565	0.084	0.185393	0.045	0.967	1098.10	0.84	1096.95	0.56	1096.37 0.45
z5	0.795	15.3708	0.9993	470	0.89	26480	0.241	0.0760872	0.042	1.94489	0.084	0.185388	0.045	0.974	1097.37	0.84	1096.68	0.56	1096.34 0.45
z1	0.714	21.4970	0.9992	415	1.38	23809	0.216	0.0760841	0.043	1.94467	0.085	0.185375	0.046	0.959	1097.29	0.87	1096.61	0.57	1096.27 0.46
z6	0.624	12.4836	0.9992	392	0.83	22979	0.189	0.0760958	0.039	1.94559	0.083	0.185339	0.045	0.991	1097.59	0.78	1096.58	0.56	1096.08 0.46
z4	0.610	11.0228	0.9988	272	1.05	15998	0.185	0.0761063	0.045	1.94483	0.087	0.185336	0.046	0.952	1097.87	0.91	1096.66	0.59	1096.06 0.47
z3	0.669	4.5808	0.9983	192	0.63	11152	0.203	0.0761323	0.055	1.94542	0.094	0.185329	0.048	0.898	^{1098.55}	^{1.11}	^{1096.87}	^{0.63}	1096.02 0.48
weighted mean ²⁰⁶ Pb/ ²³⁸ U age = 1096.19 ± 0.19 (0.36) [1.15] Ma (2s); MSWD = 0.45 (n=6)																			
<i>FC-4b Forest Center anorthosite</i> (Duluth Complex anorthosite series)																			
z8	0.775	25.2049	0.9996	894	0.76	50552	0.235	0.0760449	0.041	1.94440	0.084	0.185445	0.047	0.966	1096.25	0.82	1096.52	0.56	1096.65 0.47
z9	0.708	1.9147	0.9951	65	0.78	3759	0.214	0.0759136	0.093	1.93976	0.140	0.185322	0.073	0.794	1092.79	1.87	1094.92	0.94	1095.98 0.73
z10	0.732	8.7414	0.9986	233	1.01	13304	0.222	0.0760627	0.047	1.94330	0.089	0.185297	0.047	0.946	1096.72	0.94	1096.14	0.60	1095.85 0.47
z2	0.686	30.2158	0.9996	721	1.11	41626	0.208	0.0761076	0.041	1.94443	0.084	0.185295	0.046	0.968	1097.90	0.82	1096.53	0.56	1095.84 0.47
z4	0.705	20.9839	0.9995	610	0.92	35079	0.214	0.0761032	0.042	1.94413	0.085	0.185277	0.047	0.963	1097.79	0.83	1096.42	0.57	1095.74 0.48
z11	0.716	11.7511	0.9989	288	1.09	16503	0.217	0.0760929	0.045	1.94376	0.087	0.185266	0.046	0.954	1097.51	0.90	1096.30	0.58	1095.68 0.47
z3	0.637	48.5088	0.9998	1280	0.99	74775	0.193	0.0761148	0.040	1.94431	0.086	0.185265	0.051	0.957	1098.09	0.81	1096.48	0.58	1095.68 0.51
z1	0.630	18.1802	0.9994	548	0.87	32063	0.191	0.0760777	0.042	1.94321	0.084	0.185251	0.045	0.969	1097.12	0.84	1096.11	0.56	1095.60 0.46
z6	0.659	12.0405	0.9992	397	0.80	23077	0.199	0.0760863	0.044	1.94314	0.086	0.185223	0.047	0.955	1097.34	0.87	1096.08	0.58	1095.45 0.48
z5	0.467	9.6852	0.9988	256	0.95	15587	0.141	0.0761585	0.046	1.94327	0.088	0.185060	0.046	0.952	1099.24	0.92	1096.13	0.59	1094.56 0.47
weighted mean ²⁰⁶ Pb/ ²³⁸ U age = 1097.71 ± 0.17 (0.35) [1.14] Ma (2s); MSWD = 0.38 (n=8)																			
<i>FC-1 Forest Center anorthosite</i> (Duluth Complex anorthosite series)																			
z21	0.347	89.3479	0.9999	4055	0.54	254586	0.105	0.0761142	0.040	1.94544	0.086	0.185375	0.051	0.958	1098.08	0.80	1096.87	0.58	1096.27 0.51
z23	1.362	38.6752	0.9998	1969	0.60	97907	0.412	0.0761283	0.040	1.94564	0.086	0.185360	0.050	0.959	1098.45	0.81	1096.95	0.57	1096.19 0.51
z22	0.614	135.1333	1.0000	8332	0.42	489236	0.186	0.0760948	0.040	1.94434	0.086	0.185317	0.051	0.958	1097.56	0.80	1096.50	0.57	1095.96 0.51
z26	1.443	63.5688	0.9999	4620	0.43	225979	0.437	0.0761149	0.040	1.94485	0.084	0.185317	0.048	0.965	1098.09	0.80	1096.67	0.56	1095.96 0.48
z20	1.508	98.5654	0.9999	4740	0.66	228892	0.457	0.0761327	0.040	1.94529	0.093	0.185315	0.062	0.944	1098.56	0.80	1096.82	0.62	1095.95 0.63
z25	0.684	41.1099	0.9998	2139	0.51	123514	0.207	0.0761295	0.040	1.94493	0.083	0.185289	0.046	0.970	1098.48	0.80	1096.70	0.56	1095.81 0.47
z19	0.715	125.9011	0.9999	5523	0.61	316069	0.217	0.0761253	0.040	1.94446	0.085	0.185255	0.049	0.961	1098.37	0.80	1096.54	0.57	1095.62 0.50
z27	0.547	56.2585	0.9998	1614	0.89	96360	0.166	0.0761425	0.040	1.94490	0.084	0.185254	0.047	0.968	1098.82	0.81	1096.69	0.56	1095.62 0.47
z18	1.414	46.2410	0.9998	1865	0.77	91792	0.428	0.0761037	0.040	1.94366	0.084	0.185230	0.048	0.965	1097.80	0.81	1096.26	0.57	1095.49 0.48
z24	1.439	92.3175	0.9999	6768	0.43	331313	0.436	0.0761075	0.040	1.94349	0.085	0.185206	0.049	0.962	^{1097.90}	^{0.80}	^{1096.20}	^{0.57}	1095.35 0.50
weighted mean ²⁰⁶ Pb/ ²³⁸ U age = 1095.81 ± 0.16 (0.34) [1.14] Ma (2s); MSWD = 1.44 (n=10)																			
<i>BEI Bald Eagle intrusion</i> (Duluth Complex layered series)																			
z4	0.681	16.1663	0.9991	341.8	1.25	19772	0.206	0.0760969	0.044	1.94481	0.085	0.185357	0.044	0.966	1097.62	0.87	1096.66	0.57	1096.17 0.45
z6a	0.649	30.1146	0.9997	914	0.86	53261	0.197	0.0760783	0.045	1.94407	0.085	0.185332	0.045	0.942	1097.13	0.91	1096.40	0.57	1096.04 0.46
z6b	0.841	24.9060	0.9996	803	0.85	44740	0.255	0.0760813	0.039	1.94401	0.084	0.185319	0.048	0.974	1097.21	0.79	1096.38	0.56	1095.97 0.48
z5	0.652	4.7525	0.9983	186	0.67	10867	0.197	0.0760617	0.050	1.94340	0.090	0.185308	0.046	0.942	1096.70	0.99	1096.17	0.61	1095.91 0.46
z3	0.576	6.7271	0.9982	178	0.97	10592	0.174	0.0761041	0.052	1.94433	0.091	0.185294	0.046	0.928	1097.81	1.04	1096.49	0.61	1095.83 0.46
z1	0.523	5.9782	0.9981	159	0.96	9575	0.158	0.0761187	0.054	1.94367	0.095	0.185195	0.050	0.912	^{1098.19}	^{1.07}	^{1096.26}	^{0.64}	1095.29 0.50
weighted mean ²⁰⁶ Pb/ ²³⁸ U age = 1095.89 ± 0.19 (0.36) [1.15] Ma (2s); MSWD = 1.59 (n=6)																			
<i>HCT Houghtaling Creek troctolite</i> (Beaver Bay Complex)																			
z7	0.765	11.6934	0.9978	149	2.12	8437	0.232	0.0761478	0.055	1.94513	0.094	0.185263	0.046	0.920	1098.96	1.10	1096.77	0.63	1095.66 0.47
z6	0.666	4.7620	0.9968	101	1.24	5877	0.202	0.0760881	0.067	1.94350	0.106	0.185254	0.051	0.870	1097.39	1.34	1096.21	0.71	1095.61 0.52
z1	0.396	3.7022	0.9945	54	1.68	3382	0.120	0.0760085	0.099	1.94086	0.139	0.185196	0.060	0.784	1095.29	1.98	1095.30	0.93	1095.30 0.60
z10	0.719	3.5063	0.9965	94	1.00	5380	0.218	0.0761151	0.069	1.94320	0.108	0.185159	0.051	0.865	1098.10	1.39	1096.10	0.73	1095.10 0.51
z4	1.566	1.3175	0.9976	31	1.36														

Table DR2. Site level paleomagnetic data

site	site lat	site lon	n	dec _{is}	inc _{is}	dec _{tc}	inc _{tc}	k	α_{95}	VGP lat	VGP lon
FC1 (AF)	47.7826	-91.3265	9	301.6	40.5	297.1	52.4	32	9.3	41.3	185.0
FC1 (thermal)	47.7826	-91.3265	9	289.7	34.4	284.1	45.1	64	6.5	28.6	187.8
FC4 (AF)	47.7625	-91.3827	7	296.0	26.8	292.6	38.3	59	7.9	30.8	177.4
HCT1 (AF)	47.6008	-91.1495	7	287.2	35.6	281.0	46.0	54	8.3	26.9	190.8
HCT1 (thermal)	47.6008	-91.1495	6	285.7	45.3	276.3	55.3	144	5.6	29.5	201.0
1 (Beck layered)	46.68	-92.24	4	279.5	47.5	287.7	64.4	51	9.8	42.0	205.2
3 (Beck layered)	46.68	-92.24	4	292.0	26.5	298.0	41.9	17	17.2	36.3	175.6
4 (Beck layered)	46.68	-92.24	3	279.5	36.0	284.5	53.0	20	18.0	33.0	193.5
5 (Beck layered)	46.68	-92.24	3	279.5	55.0	291.8	71.7	14	22.0	48.4	217.4
6 (Beck layered)	46.68	-92.24	1	280.5	32.0	285.0	48.9			31.1	189.7
7 (Beck layered)	46.68	-92.24	5	278.0	33.0	282.0	50.1	85	6.8	29.7	192.7
8 (Beck layered)	46.68	-92.24	7	290.5	43.0	301.6	58.3	345	2.8	47.5	189.4
9 (Beck layered)	46.68	-92.23	3	281.5	42.0	288.7	58.7	35	13.6	39.2	197.0
10 (Beck layered)	46.70	-92.23	3	297.5	30.5	305.6	44.9	15	21.2	43.0	172.0
11 (Beck layered)	46.70	-92.22	1	284.0	30.5	289.2	47.0			32.9	185.6
12 (Beck layered)	46.72	-92.21	5	284.5	36.0	291.1	52.4	43	9.6	37.1	188.9
13 (Beck layered)	46.69	-92.24	6	281.5	28.0	285.6	44.8	437	2.7	29.3	186.4
14 (Beck layered)	46.72	-92.20	7	287.0	35.0	294.1	51.1	334	2.9	38.4	185.8
15 (Beck layered)	46.73	-92.21	2	290.0	31.5	296.9	47.2			38.2	180.4
17 (Beck layered)	46.74	-92.19	3	279.5	37.0	284.7	54.0	80	9.1	33.8	194.3
19 (Beck layered)	46.75	-92.19	4	288.0	35.0	295.3	50.9	51	9.8	39.2	184.8
20 (Beck layered)	46.77	-92.15	3	282.0	33.0	287.1	49.7	444	3.8	33.0	189.1
25 (Beck layered)	46.78	-92.12	1	273.5	18.5	274.9	36.0			17.7	188.5
27 (Beck layered)	46.77	-92.15	1	310.0	40.5	324.6	51.6			59.4	162.2
30 (Beck layered)	46.77	-92.14	1	284.0	36.5	290.6	53.0			37.1	189.8
32 (Beck layered)	46.77	-92.14	1	290.0	36.0	298.2	51.6			41.5	183.5
33 (Beck layered)	46.77	-92.15	2	288.0	32.0	294.5	48.0			37.0	182.7
35 (Beck layered)	46.79	-92.23	8	290.0	23.5	294.9	39.3	194	3.6	32.9	176.1
36 (Beck layered)	46.78	-92.21	2	276.0	27.0	278.6	44.3			24.3	190.6
37 (Beck layered)	46.79	-92.25	2	273.0	29.0	275.0	46.5			23.1	194.3
92 (Beck layered)	46.81	-92.10	3	290.0	41.5	300.2	57.0	16	20.1	45.9	188.3
93 (Beck layered)	46.83	-92.18	5	284.5	24.5	288.6	41.0	151	5.1	29.4	181.7
94 (Beck layered)	46.85	-92.04	4	291.0	36.5	299.6	51.9	107	6.8	42.7	182.9
97 (Beck layered)	46.78	-92.12	2	281.0	28.5	285.0	45.4			29.2	187.2
98 (Beck layered)	46.77	-92.13	6	288.5	34.0	295.7	49.9	115	5.3	38.8	183.6
99 (Beck layered)	46.77	-92.12	3	287.0	35.0	294.1	51.1	39	13.0	38.4	185.8
103 (Beck layered)	46.75	-92.18	2	276.0	29.0	278.8	46.3			25.5	191.8
215 (Beck layered)	48.08	-90.77	2	281.0	48.0	290.2	64.7			44.4	204.8
217 (Beck layered)	46.79	-92.20	5	287.0	41.0	296.0	57.0	53	8.6	43.0	190.8
218 (Beck layered)	46.79	-92.18	6	284.5	27.5	289.2	44.0	62	7.3	31.3	183.3
219 (Beck layered)	46.79	-92.17	5	284.5	33.5	290.5	49.9	10	19.7	35.3	187.1
220 (Beck layered)	46.80	-92.15	5	284.0	30.5	289.2	47.0	291	3.7	32.9	185.6
221 (Beck layered)	46.79	-92.14	5	290.5	27.5	296.4	43.2	1433	1.7	35.8	177.6
18 (Beck anorthosite)	46.75	-92.17	7	279.0	37.5	284.1	54.5	91	5.5	33.7	195.2
21 (Beck anorthosite)	46.77	-92.15	2	290.0	42.0	300.5	57.5			46.3	188.8
22 (Beck anorthosite)	46.78	-92.12	6	275.0	40.5	279.1	57.8	10	17.8	32.6	201.4
23 (Beck anorthosite)	46.78	-92.12	2	295.5	39.5	306.5	54.0			48.5	180.6
26 (Beck anorthosite)	46.77	-92.15	2	309.5	43.5	325.8	54.5			61.9	165.6
31 (Beck anorthosite)	46.77	-92.14	1	278.0	33.0	282.0	50.1			29.7	192.7
38 (Beck anorthosite)	46.83	-92.11	2	262.0	33.0	260.9	50.6			16.7	206.2
40 (Beck anorthosite)	46.83	-92.09	2	309.0	35.0	320.7	46.6			54.0	160.2
101 (Beck anorthosite)	46.76	-92.16	2	296.5	37.5	306.9	51.9			47.6	177.7
102 (Beck anorthosite)	46.75	-92.18	1	275.0	29.0	277.6	46.4			24.7	192.7
222 (Beck anorthosite)	46.76	-92.15	5	270.5	43.0	273.0	60.6	75	7.3	30.7	207.6

Notes: n-number of samples analyzed and included in the site mean; dec-mean declination for the site (is = insitu; tc = tilt-corrected); inc-mean inclination for the site; k=Fisher precision parameter; α_{95} =95% confidence limit in degrees; VGP lat=latitude of the virtual geomagnetic pole for the site; VGP lon=longitude of the virtual geomagnetic pole for the site. Sites in **bold** were included in the calculation of the mean pole (filtered for $\alpha_{95} < 15^\circ$ and so that only one site for FC1 and HCT). The resulting mean pole is: 188.7°E, 35.6°N, N=24, A₉₅=3.1, k=92.